Uninterruptible DC-powered boost differential inverter with a Sensor-less Changeover system

CANDIDUS U. EYA[1], AYODEJI OLALEKAN SALAU[2], STEPHEN EJIOFOR OTI[3]

[1] Department of Electrical Engineering, University of Nigeria, Nsukka, NIGERIA
[2] Department of Electrical/Electronics and Computer Engineering, Afe Babalola University, Ado-Ekiti, NIGERIA
[3] Department of Electrical Engineering, University of Nigeria, Nsukka, NIGERIA

Abstract: - This paper presents the design and implementation of an Uninterruptible DC-powered boost differential inverter with a sensor-less Changeover system. The systems design was developed using solar panels, bidirectional converter current linked battery banks, and a single-staged DC/AC Converter. The system was designed, modeled, and simulated using MATLAB/Simulink software before its implementation. The properties exhibited by the system include: Single stage input voltage transformation and amplification without a power transformer, lightweight sensor-less and relay-less automatic changeover, and a simplified feedback system. The simulation results show that the system gives a pure sine voltage and current waveforms, total harmonic distortion (THD) of 1.25%, efficiency of 94.4%, relatively fast dynamic response and 1 kilowatt power rating. The specific target areas of applications are: in medical paraphernalia where pure sine waveforms are needed, homes, and medium scale industries.

Key-Words: - Boost differential, Bidirectional Converter, Uninterruptible DC-power, Single stage, Sensor-less, pure sinewave, relay-less automatic, total harmonic distortion.

Received: August 23, 2020. Revised: December 16, 2020. Accepted: January 5, 2021. Published: January 18, 2021.

1 Introduction

The unequal provision of resources such as constant electricity supply, good road network, quality health care delivery, and adequate security policies to the rural areas as compared to the urban areas in developing countries has brought about the quest for rural-to-urban migration and high demand of individuals leaving their country to another. In the same vein, Farmer products such as tomatoes and other perishable commodities are wasted and a colossal amount of financial income is lost; thus the need for an alternative means of power generation. More recently, these farm products are being preserved with the aid of newly developed power electronic system appliances. These appliances are environmentally friendly, thereby making the dependency on fossil fuels a thing of past.

It is common knowledge that inadequate power supply results in low productivity and slow economic development. This challenge has made investors shift their attention to the urban areas. Similarly, this has also created a chain of other challenges such as hardship and high rate of crime. In Nigeria for instance, utilities, power infrastructure, and power supply are in shambles which has caused Nigeria to loss about 474 billion naira annually [1, 2]. This challenge amongst numerous has made it impossible for Nigeria Electricity supply industry to supply enough power to people living in urban areas, let alone to supply sufficient electricity to the remote/rural areas. Eventually, when the electricity challenge is addressed, it would bring about steady, clean, and conditioned power supply, thereby encourages investors, promoting a pollution-free environment, and in turn raise the standard of living [3]. In developed countries, alternative/uninterruptible power supplies are ubiquitous, thus eliminating prolonged power interruptions or total blackout to the utility subscribers. This has encouraged many investors to invest in such regions, leading to reduced cost of living and improved economy. Numerous research efforts have been directed in the area of uninterruptible power supplies (UPS) and changeover systems with different merits and

demerits [4]. USP systems have found applications in many areas where uninterrupted power supply is a necessity [5]. There are many classifications of UPS such as OFF-line UPS, ON-line UPS and Line interactive UPS. In OFF-line UPS, the inverter is normally set OFF [6]. The connected loads are fed from the mains utility supply. Once the mains supply is not accessible, a static power switch switches on the inverter and connects it to the load automatically. When the supply is brought back, the inverter is again shut off. The problem with the OFF-line UPS is that they are interrupted momentarily each time the utility supply fails.

In most cases, uninterruptible power supplies are known to change from one AC power source to another AC power source or from AC power source to DC/AC power source in order to maintain stable power to the connected loads in case of any interruption on the actively supplying end. For instance, if utility power is suddenly off under UPS state, the loads are meant to be connected to a stand-by AC generator or the output of inverter system (DC/AC power system) in an uninterruptible power supply system between utility power supply and DC/AC system network.

This paper presents a DC-powered boost differential inverter for the purpose of uninterruptible power supply to the remotest rural areas where there is no grid-utility power supply and lack of stand-by AC generators at DC voltage buses in the system. This was achieved by the combination of two DC power sources that energize DC-AC converter to deliver constant and reliable power supply to rural dwellers. The DC-AC converter that is adopted in this work is known as boost differential inverter which has been used by authors in [7-10] but not in this area of research work. The DC-AC converter is powered by alternatively connecting one solar-DC power network to two-arm (double network) battery banks [11]. The solar-DC power network converts solar energy into electrical energy, whereas battery banks convert chemical energy into electrical energy. This shows that there is interaction between solar energy, electrical energy, and chemical energy to accomplish a particular purpose of constant DC power supply to an inverter input rail. During a changeover situation, there is no sensor and relay system for changing from one source to another is needed. The changeover depends on the difference in voltage between the solar panels and the battery network system. This happens at micro time scale, unlike the AC power changeover system, in which the voltages between the two power sources are equal and both combine together to power the connected load(s). In this study, DC power from solar panel modules (as the primary power supply) and two-48V parallel connected-battery banks (as the secondary power supply) are linked together with the aid of bidirectional DC-DC converters which provide constant DC-power supply to portable DC-AC boost converters without sensor and changeover relay switch systems. This implies that when the DC power is lower than the DC power from battery systems, it will automatically changeover to double-battery bank systems with sensor-less system. Also once a steady power is maintained and the feedback system is functional, the output voltage of the boost differential inverter becomes constant. This will lead to a steady power supply to the rural dwellers and other critical loads in the villages such healthcare centers.

2 Proposed System

The Photovoltaic (PV) arrary in Fig. 1 converts the solar energy from the sun into useful electrical energy to feed the load through the inverter and charge the two battery banks.

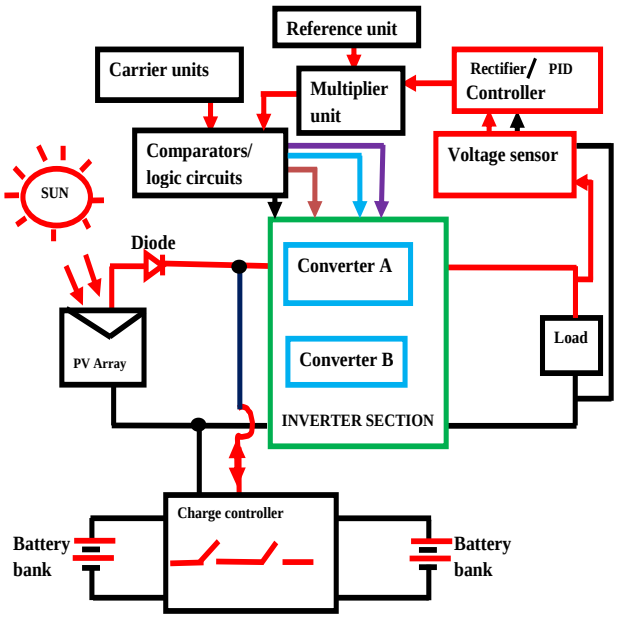

Fig. 1. Block diagram of the designed system.

In cases where the PV voltage is lower than the battery voltage, the battery will deliver power to the load automatically. But when they have the same potential difference, they both feed the load and at that point in time, their currents jointly flow to the load since the load has lower potential. This means

that during the day there will be always constant DC voltage at the DC bus system.

The voltage sensor at the output of the inverter system has nothing to do with the changeover sytem between the two power sources. It monitors the output AC voltage level across the resistor-inductor-capacitor (RLC) load. When the AC voltage is less than or more than 230V rms, it sends a signal to the logic control unit (signal rectifier, PID controller, multiplier, reference, carrier wave, comparators) to stabilize the output voltage of the system by adjusting the witdth of the triggering pulses. The power circuit block diagram in Fig. 1 is represented as a circuit diagram in Fig. 2.

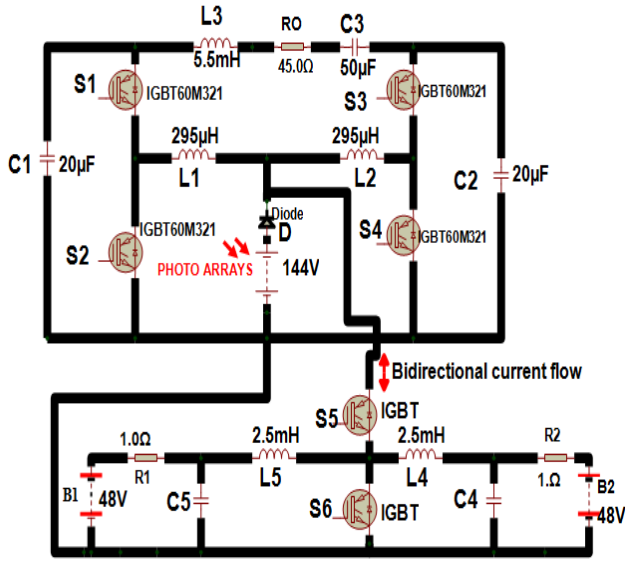

Fig. 2. Power circuit of the designed system.

Fig. 2 consists of photo arrays (144V DC series-parallel connected cells), power diode for unidirectional current flow, boost differential inverter (Insulated gate bipolar transistors (IGBT60M321)), power switches S1, S2, S3, S4, inductors L1, L2, capacitors C1, C2, RLC loads, and two-arm battery banks. The differential inverter boost and changes DC power to AC power at a desired voltage and current in a single stage power conversion. This increases the efficiency and also reduces the power losses in the system. The two-arm battery bank system stores chemical energy when the energy from the solar panels is surplus. When the electrical energy goes low, the battery converts the chemical energy back to electrical energy to feed the load. The current from the battery does not flow back to the solar panel due to the presence of power diode, D.

3 Analysis of the Proposed System

3.1 Photo Arrays

Fig. 3(a) displays a simplified PV circuit of photo arrays which convert the solar energy into electrical energy depending on the intensity of the sun's radiation.

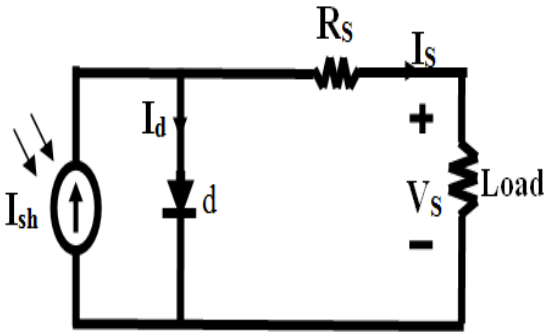

Fig. 3a. The Photovoltaic (PV) cell model without shunt resistance.

The Eq. (1) depicts the current-voltage relationship of a PV cell [12].

$$I_S = \boldsymbol{I_{sh}} - I_d = I_{sh} - I_o\left(e^{q(V+I_S R_S)/nkT} - 1\right) \qquad (1)$$

where I_S is the cell current (the same as the module current), V is the cell voltage. V is the ratio of module voltage to number of cells in series, T is the cell temperature in Kelvin (K), n is the ideality factor of the diode ($1 \leq n \leq 2$), q is the Electronic charge, V_{oc} is the open circuit voltage, k is the Boltzmann's constant, and I_o is the reverse saturation current of the diode.

It is very vital to bear in mind that temperature, resistance, dust, shadow, irradiation, and angle placement of solar panels affect its output power and should be taken into consideration.

3.1.1 Modeling of the system: Photo Array, Inverter, and Battery systems

Fig. 3(b) shows the photo array model used in this work. One of the solar panels used NS-F135G5 Sharp Amorphous which has a short circuit current, I_{sc} = 3.40A, open circuit voltage, V_{oc} = 61V, maximum current at standard temperature condition

STC, I_{mp} = 2.88A, and maximum voltage, Vp_{max} = 48.0V.

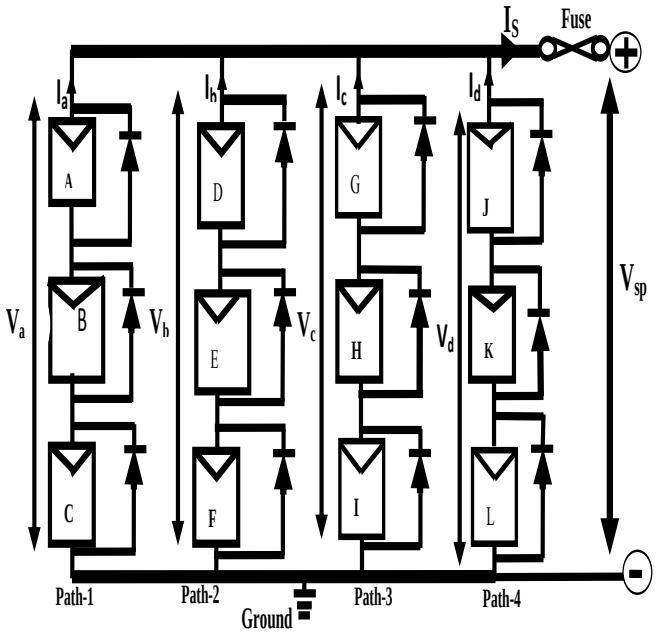

Fig. 3b. Photo array model.

This does not give the required voltage and current needed in this work. Therefore, we combined the solar panels in a series-parallel form to actualize our aim as shown in Fig. 3(b).

The equations of the models output current and voltage are given in Eqs. (2) and (3) according to Kirchhoff's current and voltage laws.

$$I_S = I_a + I_b + I_c + I_d \tag{2}$$

$$V_{sp} = V_b = V_D + V_E + V_F \tag{3}$$

where $I_a, I_b, I_c,$ and I_d are currents along paths 1, 2, 3, and 4. The $V_a, V_b, V_c,$ *and* V_d are the voltages across path 1, 2, 3, and 4 and are of the same value. The V_D, V_E, and V_F are individual voltages of solar panel connected in series along path 2.

Fig. 4 shows a simplified circuit current diagram of the proposed system when the output solar panel voltage, Vsp (Vs) > V_B ($V_{B1} = V_{B2}$), battery network voltage. Under this condition, the solar panel output feeds the inverter section and charges both battery banks.

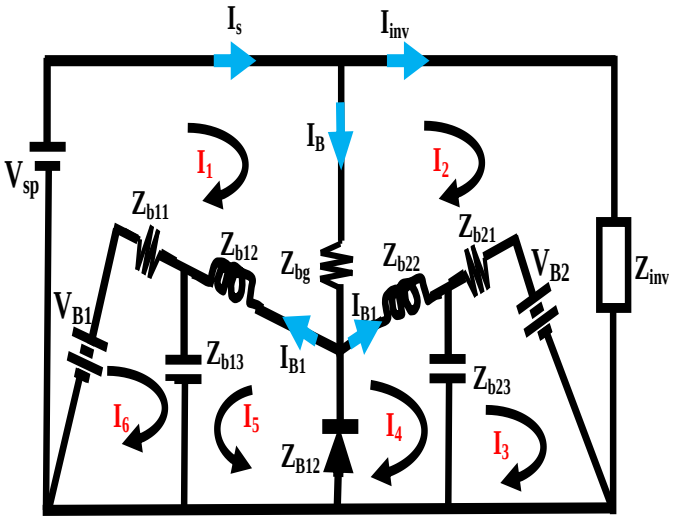

Fig. 4. Current circuit diagram of proposed system , if Vs > V_B.

The output current of the solar panel I_s, input current of the inverter I_{inv}, and battery charging current I_B, are related as given by Eq. (4).

$$I_s = I_{inv} + (I_B) \tag{4}$$

The Eq. (5) represents the relationship between the voltages, (Vsp,V_{B1}) and loop currents I_1, I_2, I_3, I_4, I_5, I_6, and branch impendences of the system once Vsp > V_{B1} *or* V_{B2}.

$$\begin{bmatrix} V_{sp} \\ V_{B2} \\ -V_{B2} \\ 0 \\ 0 \\ V_{B1} \end{bmatrix} = \begin{bmatrix} -I_1 \\ I_2 \\ -I_3 \\ -I_4 \\ I_5 \\ I_6 \end{bmatrix} \begin{bmatrix} Z_{bg}+Z_{b12}+Z_{b11} & -Z_{bg} & 0 & 0 & -Z_{b12} & -Z_{b11} \\ -Z_{bg} & Z_{inv}+Z_{B2}+Z_{b21}+Z_{b21} & -Z_{b21} & -Z_{b22} & 0 & 0 \\ 0 & -Z_{b21} & Z_{bg}+Z_{b12} & -Z_{b23} & 0 & 0 \\ 0 & -Z_{b22} & -Z_{b23} & Z_{22}+Z_{b23} & -Z_{12} & 0 \\ -Z_{12} & 0 & 0 & -Z_{B12} & Z_{B12}+Z_{b12}+Z_{b13} & -Z_{13} \\ -Z_{b11} & 0 & 0 & 0 & -Z_{b13} & Z_{B12}+Z_{b12} \end{bmatrix} \tag{5}$$

when the solar panel voltage, Vs (Vsp) < V_{B1} *or* V_{B2}, the two battery banks jointly discharge to feed the inverter but current does not flow to the photo arrays due to the presence of unidirectional power diode, D. The expression for the relationship between I_s, I_{inv} and I_B, becomes

$$I_{inv} = (-I_B) + I_s \tag{6}$$

But since Vs < V_B then, I_s becomes extremely small and can be ignored.

Then, Eq. (6) can be written as

$$I_{inv} = -I_B \tag{7}$$

$$\begin{bmatrix} V_{sp} \\ V_{B2} \\ -V_{B2} \\ 0 \\ 0 \\ V_{B1} \end{bmatrix} = \begin{bmatrix} I_1 \\ I_2 \\ I_3 \\ I_4 \\ -I_5 \\ I_6 \end{bmatrix} \begin{bmatrix} Z_{bg}+Z_{b12}+Z_{b11} & -Z_{bg} & 0 & 0 & -Z_{b12} & -Z_{b11} \\ -Z_{bg} & Z_{inv}+Z_{B2}+Z_{b21}+Z_{b21} & -Z_{b21} & -z_{b22} & 0 & 0 \\ 0 & -Z_{b21} & Z_{bg}+Z_{b12} & -Z_{b23} & 0 & 0 \\ 0 & -z_{b22} & -Z_{b23} & Z_{22}+Z_{b23} & -Z_{12} & 0 \\ -Z_{12} & 0 & 0 & -Z_{B12} & Z_{B12}+Z_{b12}+Z_{b13} & -Z_{13} \\ -Z_{b11} & 0 & 0 & 0 & -Z_{b13} & Z_{B12}+Z_{b12} \end{bmatrix} \tag{8}$$

Therefore, the current circuit diagram of the proposed system is shown in Fig. 5.

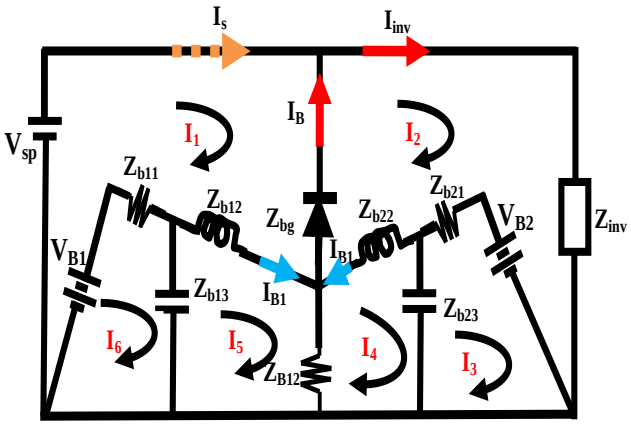

Fig. 5. Current circuit diagram of proposed system, if Vs > V_B.

As soon as Vs = V_B, the current and voltage equations of Fig. 6 become,

$$\begin{bmatrix} V_{sp} \\ V_{B2} \\ -V_{B2} \\ 0 \\ 0 \\ V_{B1} \end{bmatrix} = \begin{bmatrix} I_1 \\ I_2 \\ I_3 \\ I_4 \\ I_5 \\ I_6 \end{bmatrix} \begin{bmatrix} Z_{bg}+Z_{b12}+Z_{b11} & -Z_{bg} & 0 & 0 & -Z_{b12} & -Z_{b11} \\ -Z_{bg} & Z_{inv}+Z_{B2}+Z_{b21}+Z_{b21} & -Z_{b21} & -z_{b22} & 0 & 0 \\ 0 & -Z_{b21} & Z_{bg}+Z_{b12} & -Z_{b23} & 0 & 0 \\ 0 & -z_{b22} & -Z_{b23} & Z_{22}+Z_{b23} & -Z_{12} & 0 \\ -Z_{12} & 0 & 0 & -Z_{B12} & Z_{B12}+Z_{b12}+Z_{b13} & -Z_{13} \\ -Z_{b11} & 0 & 0 & 0 & -Z_{b13} & Z_{B12}+Z_{b12} \end{bmatrix} \tag{10}$$

3.2. Analysis and principle operation of Single Phase Boost differential inverter under R-L-C loads

Once the gate terminals of the power switches are connected and the converted electrical energy from the solar energy is impressed at DC power line of the inverter under positive cycle, the S1 and S4 are closed while S2 and S3 are turned OFF. The current flows from source voltage Vin (Vs or Vsp) and through power diode D, input inductor L1, S1, capacitor C1, and back to Vin in converter A. This current movement dischages the magnetic field energy temporarily setup in L1 to charge the

I_B is negative because it flows in the opposite direction to I_s that is charging it. Therefore, the voltage equations of the system becomes

$$I_{inv} = I_S + I_B \tag{9}$$

Therefore the voltage can be obtained using Eq. (10).

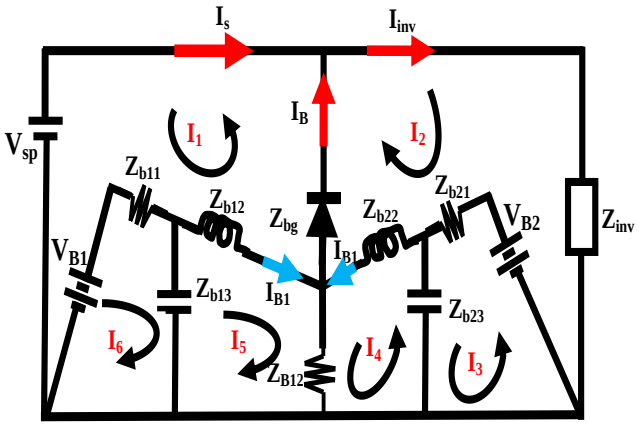

Fig. 6. current Circuit diagram of proposed system , if Vsp = V_B.

capacitor, C1. In converter B, the current flows from Vin and passes through the input inductor, L2 and S4, and back to Vin in order to linearly build up the energy in L2. In the same vein, the already stored energy in capacitor C2, feeds the load as shown in Fig. 7(a).

Fig. 7(b) shows when the system is under dead-band controlled condition. Here, no current flows to the load from any of the power source, rather the energy in C1 and C2 discharge to loads until a negative cycle takes place. During the negative half cycle, the S1 and S4 are switched OFF while S2 and S3 are ON.

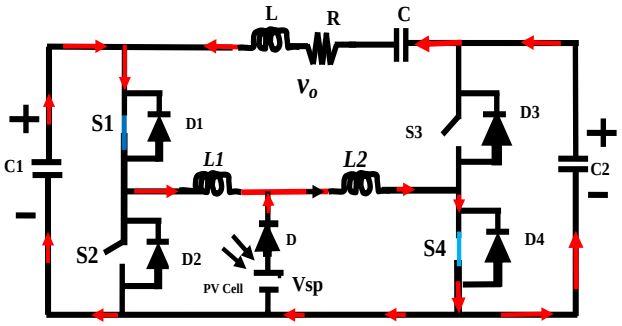

Fig. 7(a). Current flow in positive half cycle.

The current flows from source voltage Vsp and through free wheeling D, input inductor L1, S1, capacitor C1 and back to Vsp in converter A. This current movement dischages the magnetic field energy momentarily built in L1 to charge the capacitor C1.

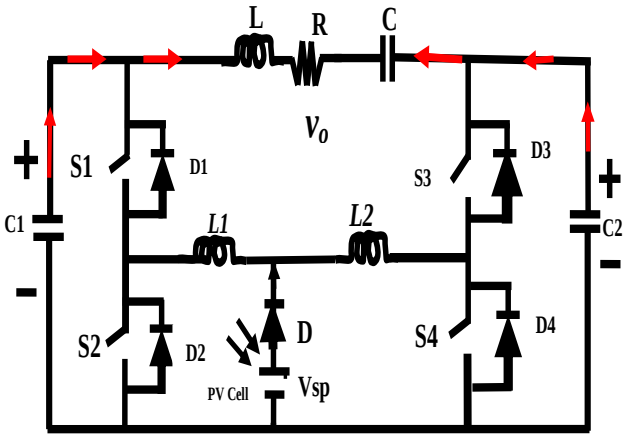

Fig. 7(b). Dead-band current flow circuit in positive half cycle.

In converter B, the current flows from Vsp and passes input inductor L2 and S4 and flows back to Vsp in order to linearly build up the energy in L2. In that instance, the already stored energy in capacitor C2, feeds the load as shown in Fig. 7(c).

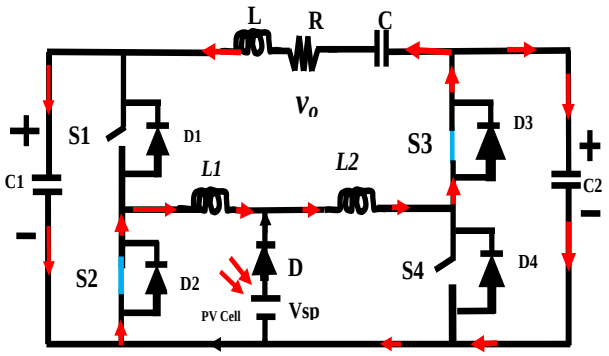

Fig. 7(c). Current flow in negative half cycle.

Before a positive cycle comes up again, the blanking period must be experienced where the load is fed by C1 and C2 only. The load voltage v_o across the RLC load is derived from two DC biased output voltage of converter A and B of the DC-AC converter with dc-offset V_{dc}, amplitude V_o, and angle of operation as follow:

$$v_A = V_{dc} + \frac{\left[V_o cos\left(\theta - \frac{\pi}{2}\right)\right]}{2} \tag{11}$$

$$v_B = V_{dc} + \frac{\left[V_o cos\left(\theta - \frac{3\pi}{2}\right)\right]}{2} \tag{12}$$

$$v_o = v_A - v_B = V_o cos\left(\theta - \frac{\pi}{2}\right) \tag{13}$$

The Eqs. (11) and (12) describe the voltage outputs of the two DC/DC converters of boost differential inverter while Eq. (13) shows the output of the boost differential inverter.

Based on the averaging concept for boost converters the voltage relationship for the continuous conduction mode (CCM) of converters A and B is determined by Eq. (14) [13].

$$v_A = v_B = \left[\frac{V_{in}}{D_c}\right] \div \left[\frac{1-D_c}{D_c}\right] \tag{14}$$

where D_c represents duty cycles of the boost converters.

The capacitances C1, C2 and inductances, $L1$, $L2$ are calculated using Eqs. (15) and (16) [13].

$$L_{min} = \frac{R(1-D_c)^2 D_c}{2f} \tag{15}$$

$$C_{min} = \frac{D_c}{Rf\left(\frac{\Delta V_o}{V_o}\right)} \tag{16}$$

where L_{min} and C_{min} are the minimum inductance and capacitance of the DC-DC converter under continuous conduction mode (CCM).

The reference signal S_{ref} and carrier waves (C_{r1} and C_{r2}) signals are generated using the expressions in Eqs. (17), (18), and (19).

$$S_{ref} = S_a sin\theta \quad (17)$$

$$C_{r1} = \begin{bmatrix} 0 & \frac{1}{2f} & \frac{3}{4f} & \frac{1}{f} \\ 0 & a_c & 0 & -a_c \end{bmatrix} \quad (18)$$

$$C_{r2} = \begin{bmatrix} 0 & \frac{1}{2f} & \frac{1}{f_c} \\ 0 & b_c & 0 \end{bmatrix} \quad (19)$$

where f is the Switching frequency of the carrier waves (C_{r1} and C_{r2}), a_c is the amplitude C_{r1}, and b_c is the magnitude of carrier wave C_{r2}.

The firing signals for switching S1, S2, S3, and S4 are produced by comparing Eqs. (17) and (18) while Eq. (19) is compared with the positive DC voltage which must be less than b_c to trigger S5 and S6.

4. Efficiency Evaluation of the Proposed System

Efficiency, ε of the system can be defined as power output of inverter per power input expressed in percent. It can be expressed based on the output power and power losses as follow:

$$\varepsilon = \frac{load\ power \times 100}{Load\ power + power\ losses} \quad (20)$$

In this research, the output power of the inverter, P_o and the power losses, P_L are considered for the efficiency evaluation. The power losses that are taken into consideration are the losses in the snubber circuit, and inductor coils as well as device loss (Conduction loss).

4.1. Losses in the Proposed System

In this system, the snubber circuits, input inductor coils and the device losses (conduction losses) are considered. Their consideration is based on the knowledge that the major losses occur in those regions. In the snubber circuit, each switch snubber charges and discharges once in a cycle. Therefore, the energy loss per cycle, E_{Ls} is given in Eq. (21) [14].

$$E_{ls} = \frac{2C_s V_s^2}{2} \quad (21)$$

For the eight switches in the whole system, the energy loss per cycle in the snubber circuits, E_{Ls} is expressed as

$$E_{ls} = \frac{16C_s V_s^2}{2} \quad (22)$$

where C_s is the capacitance of snubber capacitor, V_s is the maximum voltage from the PV, f is the switching frequency.

Then, the power loss per cycle in the eight snubber circuits, P_{Ls} is given as

$$P_{ls} = \frac{16C_s V_s^2 f}{2} \quad (23)$$

Considering the inductor coils, the inductor coil's power loss, P_{iL} is expressed as

$$P_{il} = I_{rms}^2 R_{lin} \quad (24)$$

I_{rms} is current flowing through the inductor and R_{lin} is the internal resistance of the inductor coil given as Eq. (25).

$$R_{lin} = \frac{\omega L}{Q} \quad (25)$$

ω is the angular frequency (rads/sec), L is the inductance of the inductor, Q is the quality characteristic (factor) of inductor.

Furthermore, the Conduction loss (Device loss), P_{cl} of the system is given by Eq. (26) [15, 16].

$$P_{cl} = I_{av} V_d n_d \quad (26)$$

where V_d is the voltage across the device, I_{av} is the average current flowing through the device, and n_d is the number of devices. The average current (I_{av}) flowing through the device is given by Eq. (27).

$$I_{av} = \int_0^{\pi} \left(\frac{V_{orms}}{R} sin\omega t\right) d\omega t = \frac{V_{orms}}{\pi R} \quad (27)$$

5. Results and Discussion of Simulations and Laboratory Experimentation

This work was modeled and simulated in a MATLAB/Simulink 2014 software environment. The Table 1 shows the overall characteristics of the photo array modeled in this work.

Table. 1. The Solar panels of NS-F135G5 Sharp Amorphous characteristics.

Maximum Power (P_{max})	1.70kW
Voltage at P_{max} (V_{mp})	144.00V
Current at P_{max} (I_{mp})	11.52A
Open circuit voltage (V_{oc})	183.00V
Short circuit current (I_{sc})	13.60A
Temperature coefficient of I_{sc}	0.065 ± 0.015 JmA/^{0}C
Temperature coefficient of V_{oc}	-160±20JmV/^{0}C

The current and voltage (I-V) characteristics were simulated in MATLAB M-file. This was achieved by analyzing the I-V characteristics of the solar panel, NS-F135G5 Sharp Amorphous made in Japan using the following factors: temperature, resistance, and insolation.

5.1. The Influence of Temperature on the PV Panels

The I-V characteristic of PV module at varying temperatures is graphically shown in Fig. 8.

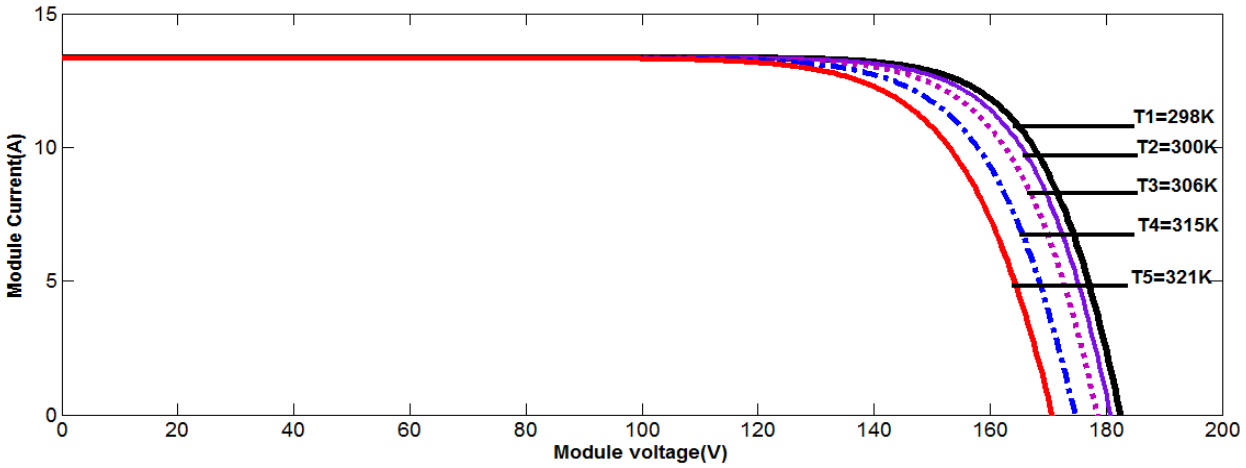

Fig. 8. The effect of temperature on the output of solar module.

Results from Fig. 8 show that the higher the temperature of the PV module, the lower the voltage and current which decreases the power output of the system and vice versa. At 321K, the current and voltage are at 5A and 138.4V, while at 298K the current and voltage are at 11.52A and 144V as observed from the knee point of the I-V curve.

5.2. The Effect of Solar Irradiation (Insolation) on the Output of Solar Module

The I-V curve of insolation is shown in Fig. 9. The graph of I-V curve of PV module indicates that the greater the insolation on the surface of the photo arrays, the more the power output (current and voltage) of the PV system. At insolation, G_5 = 0.2kW/m^2 as seen from Fig. 9.

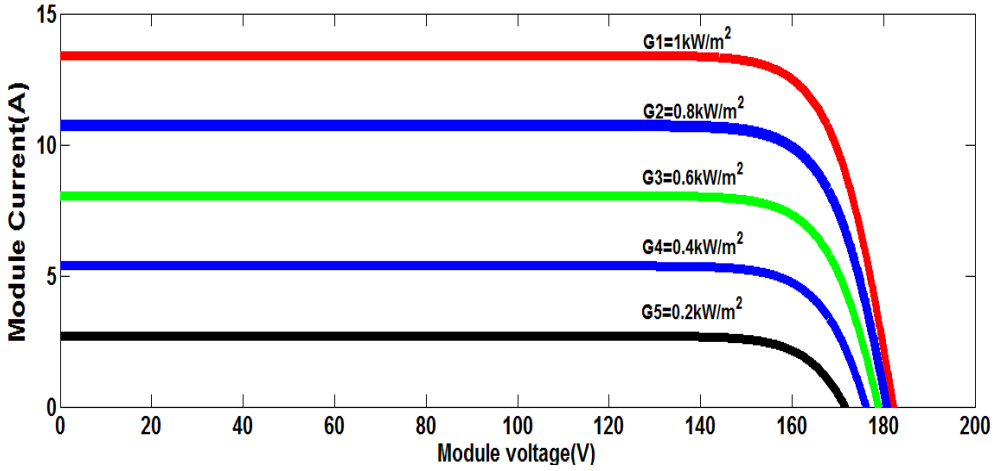

Fig. 9. The effect of solar insolation on the output of solar module.

Also the current and voltage are deduced to 2.5A and 143V, whereas at G_1 = 1kW/m^2 the current and voltage are 11.52A and 160V.

5.3. The effect of series Resistance on the output of solar module

The effects of the series resistance on I-V characteristics of PV module are shown in Fig. 10.

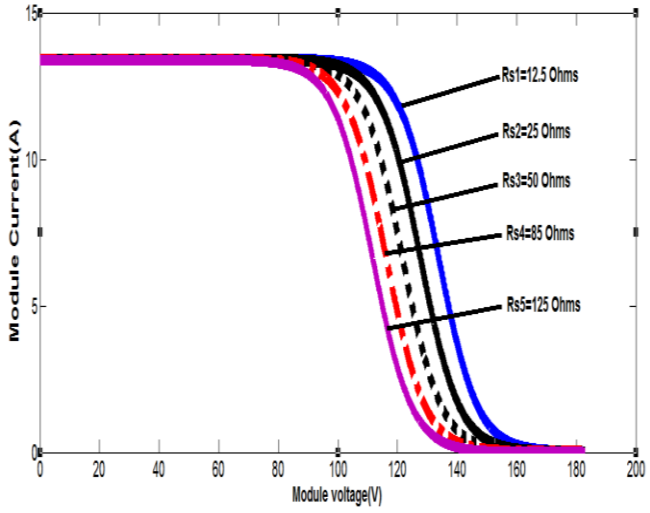

Fig. 10. The effects of the series resistance on I-V characteristics of PV module.

As series resistance increases from 12.5Ω to 125Ω, the terminal voltage starts dropping from 144V down to 90V.

The modulation scheme used in this work is shown in Fig. 11. Fig. 11(a) shows the modulating signal with amplitude of 0.8V at 50Hz. It is generated using Eq. (16), whereas Fig. 11(b) displayed the carrier wave signal with 1.0V and 20 kHz.

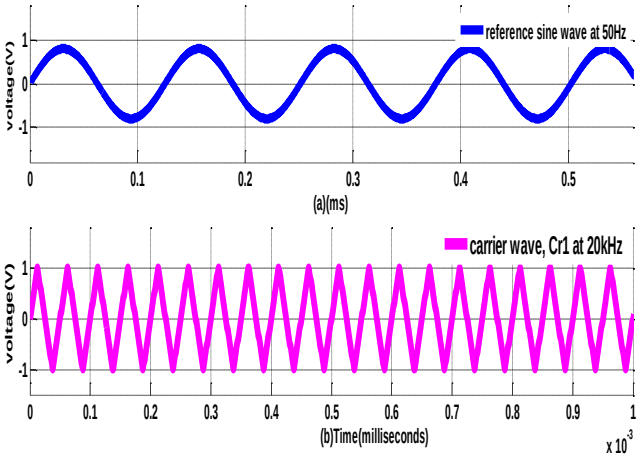

Fig. 11. (a) Reference sinewave at 50Hz (b) Carrier wave at 20 kHz.

The carrier wave signal is produced by using Eq. (17). When they are compared with each other, they produce the waveforms in Fig. 12.

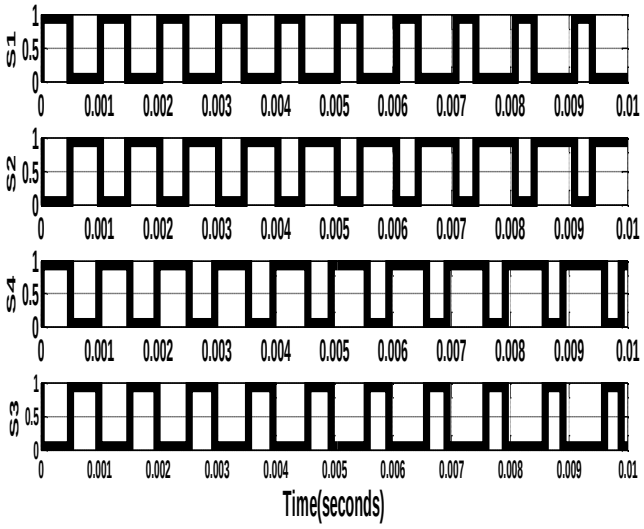

Fig. 12. Triggering gate signals of the single phase boost differential inverter.

In Fig. 12, S1 and S4 are high and low at the same time, while S2 and S3 have a similar waveform. This pattern prevails only in theory. But practically, there must be a dead band circuitry (blanking circuit) to separate the switching signals. The S1, S2, S3, and S4 signals are used for switching the boost differential inverter which converts the DC power to AC power as shown in Fig. 13.

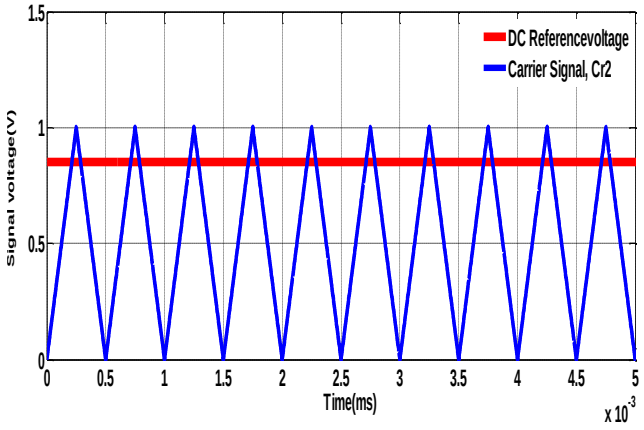

Fig. 13. DC-carrier based modulation scheme.

In order to trigger the power switches of S5 and S6, the DC-signal voltage waveform with amplitude of 0.85V is matched up with 1.0V triangular carrier waveform as shown in Fig. 13 to generate the triggering signals shown in Fig. 12. The 1.0V triangular carrier waveform in Fig. 13 is formed using Eq. (18). Fig. 14 presents the pulses for switching S5 and S6 power switches of bidirectional DC-DC converter. When S5 = ON, S6 = OFF and verse versa. It is observed that they are complementary to each other.

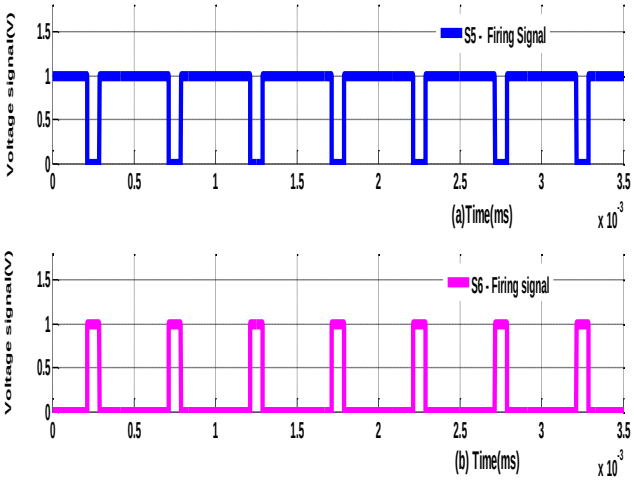

Fig. 14. Firing gate signals of the bidirectional DC-DC converter.

Fig. 15 shows the 144V maximum DC output voltage of the solar panels, 78V DC voltage being supplied from the solar panels to the inverter input terminals before the changeover. The 48V DC of the battery voltage after the changeover becomes 58V DC of charging voltage. During the period of solar panels supply to the t input of the inverter terminals DC voltage bus, the 58V DC is being used to charge the battery which is indicated by the dotted line within S-D region.

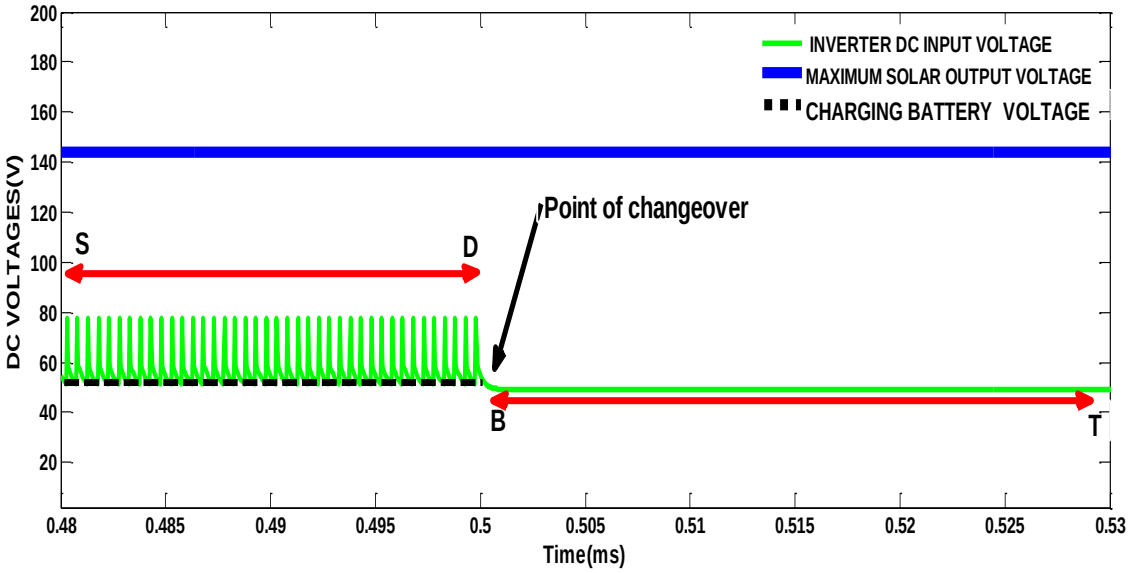

Fig. 15. Changeover pattern at Inverter input of the proposed system.

At a time interval of $0 \leq t \leq 0.5$ms and at the S-D region, the Photo arrays (solar panels) feed the DC-AC converter with 78V DC and charge the battery with 58V DC. It is observed that during the power supply from solar panels, the DC voltage from the battery is not shown at the input terminals of the inverter; thus it is not represented in the S-D region. Again at $t = 0.500005$ms, the inverter input terminals changeover to battery voltage supply and automatically give a smooth short curve between D and B, as shown in Fig. 15. The DC voltage from the solar panels ceased to appear at the input inverter terminals as shown in Fig. 15. This shows that the battery voltage is greater than the output voltage of solar panels. The inverter input DC voltage is represented with a green color in Fig. 15. This changeover situation bring about some transiency in the AC output of the inverter, but with the help of the feedback system, the inverter output voltage is restored as shown in Fig. 16(c).

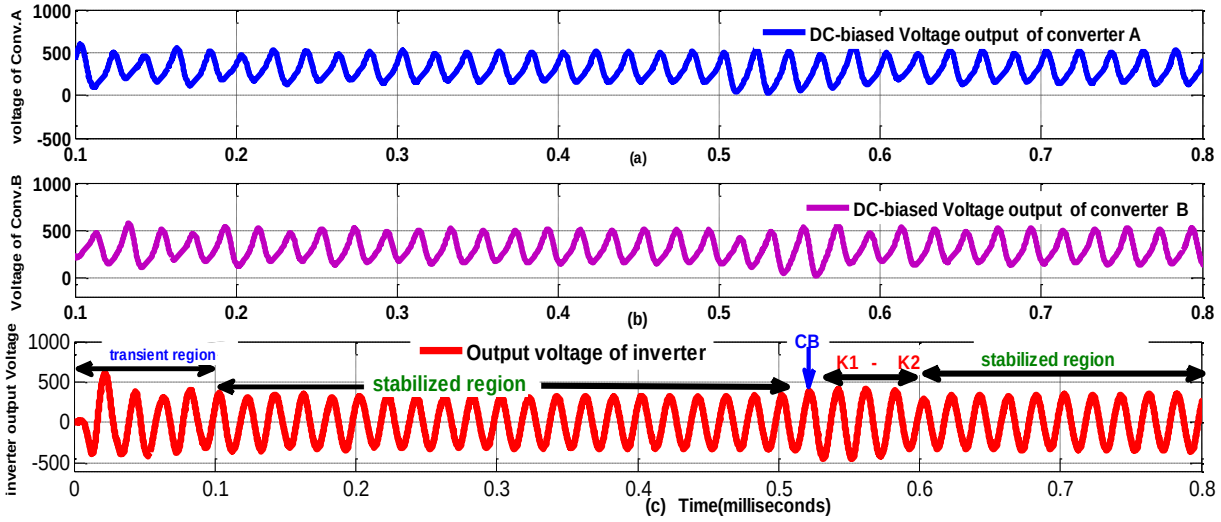

Fig. 16. (a) DC-baised voltage of Converter A. (b) DC-baised voltage of Converter B. (c) Output voltage waveform of boost differential Inverter of the proposed system.

In case the battery voltage becomes lower than the output voltage of solar panels, the reverse movement takes place. Hence, keeping a steady DC power supply at the inverter input which gives a

constant power supply at the critical loads in the remotest villages. The simulated DC-baised voltages of Converter A and B of the proposed system is stated mathematically in Eqs. (10), (11), and are represented in Figs. 16(a) and (b). The disparity between the two waveforms of Fig. 16(a) and (b) illustrates the AC output voltage of the boost differential inverter of the proposed system as illustrated in Fig. 16(c) and already expressed mathematically in Eq. (12). At time interval of $0 \leq t \leq 0.1$ms, the inverter output voltage transiently changes from 0.0V to 600V and then settles down at 325.10V due to the presence of the incorporated feedback system. The proposed systems AC output voltage remains stable at time intervals $0.1 \leq t \leq 0.5$ms. At exactly, t = 0.50005ms and point CD, there is a changeover power supply from the photo arrays (Solar panels') supply to the battery banks. This situation brings about a small AC inverter output voltage fluctuations at a time interval of $0.500005 \leq t \leq 0.6$ms and K1-K2. The AC inverter output is restored back to 325.10V at a time interval of $0.6 \leq t \leq 0.8$ ms as shown in Fig. 17.

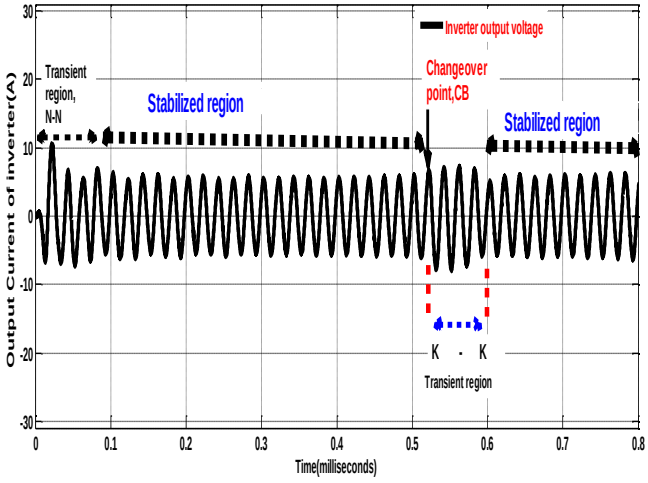

Fig. 17. Output voltage waveform of boost differential Inverter of the proposed system.

The boost differential inverter output current is displayed in Fig. 17. It mimics the behavours of the AC inverter output waveform shown in Fig. 16; the only difference is their magnitudes. At a time interval of $0 \leq t \leq 0.1$ms, the current rises from 0.0A to 12.0A, while at a time interval of $0.1 \leq t \leq 0.5$ms, it remained at 4.57A. At $0.500005 \leq t \leq 0.6$ms it varied from 4.57A to 7.76A and returns to a stable state of 4.57A. This stable state is shown in Fig. 18.

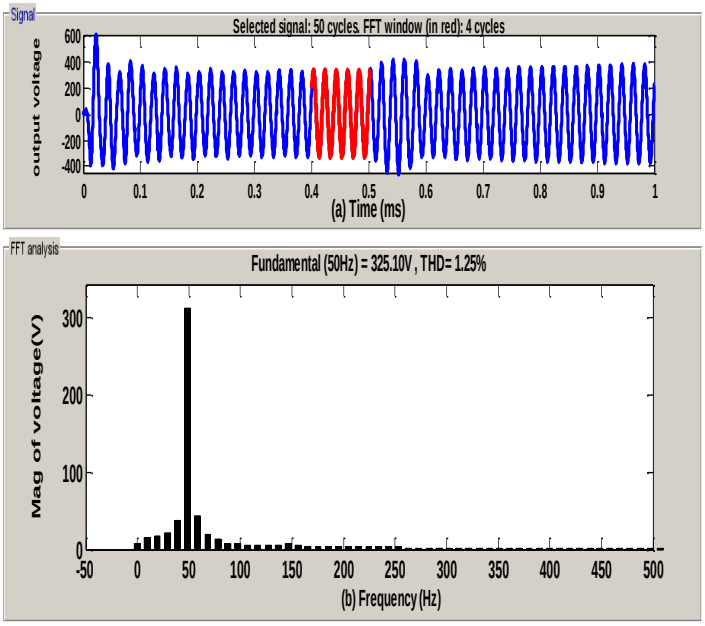

Fig. 18. Spectral characteristics of the proposed system.

Fig. 18 portrayed the spectral characteristics of the proposed system. It showed that the AC output voltage of the proposed system has peak value of 325.1V and total harmonic distortion (THD) of 1.25% at fundamental frequency of 50Hz. This implies that the power required by the system is small and the system is very efficient. The parameters obtained from the proposed system are presented in Table 2.

Table 2. Proposed system parameters

Type of inverter used	Single phase single stage boost differential Inverter
Maximum Output voltage of solar panels	144VDC
Maximum Input Current	11.52ADC
Short circuit current	13.60ADC

Open circuit voltage	183.00VDC
Switching frequencies of carriers	20kHz and 1kHz
AC output voltage (rms)	325.1V (230Vrms)
Inverter output power	1485.7W
IGBT Voltage drop	1.000V
L1 = L2 of power circuit	295µH
C1 = C2 of power circuit	20µF
Bidirectional DC-DC converter components (resistors, inductors and capacitors)	1.0Ω, 2.5mH and 1000 µF, 480V
Rms inductor Input current I_{rms}	5.60A
Load resistance, inductance and capacitance	45Ω, 5.5mH, and 50 µF
Kp	10.000
K_i	2.173
Kd	0.001
Quality factor	50.00
Total harmonic distortion (THD)	1.25%
Efficiency	94.40%

5.4. Sinewave and Triangular wave (carrier wave) Generation for the Single Phase Boost Differential Inverter

Fig. 19(a) shows an Oscilloscopic waveform of a reference sine wave. It has frequency of 50.30Hz and an amplitude of 7.8V. The laboratory frequency value is similar to the simulated 50Hz frequency as shown in Fig. 11(a).

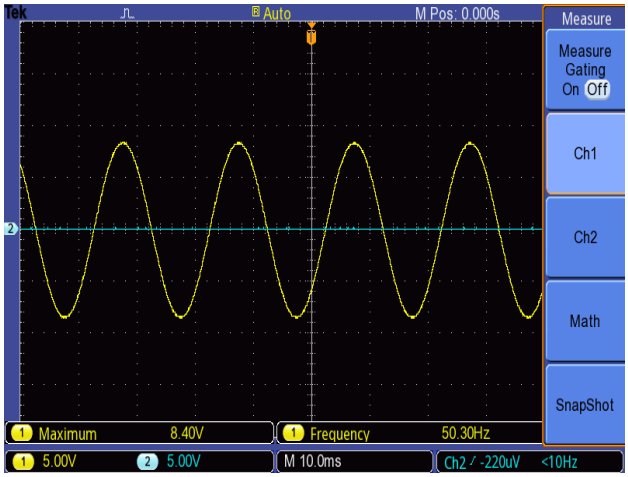

Fig. 19a. Reference sine wave.

This frequency determines the output voltage wave frequency of the boost differential inverter. The carrier wave is shown in Fig. 19(b).

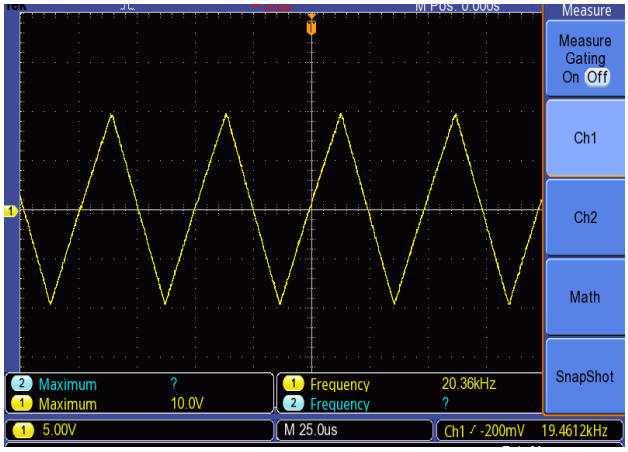

Fig. 19(b). Triangular wave (Carrier wave).

It has frequency of 20.30 kHz with a peak voltage of 10.0V. The Fig. 20 depicts the laboratory

generated sinewave and triangular waves. The waveforms are compared and gapped to generate the pulses in Fig. 20 and Fig. 21(a).

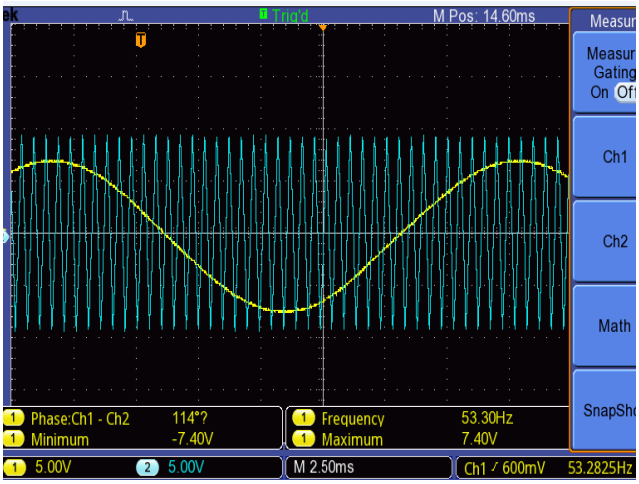

Fig. 20. Sinewave Triangular wave signals.

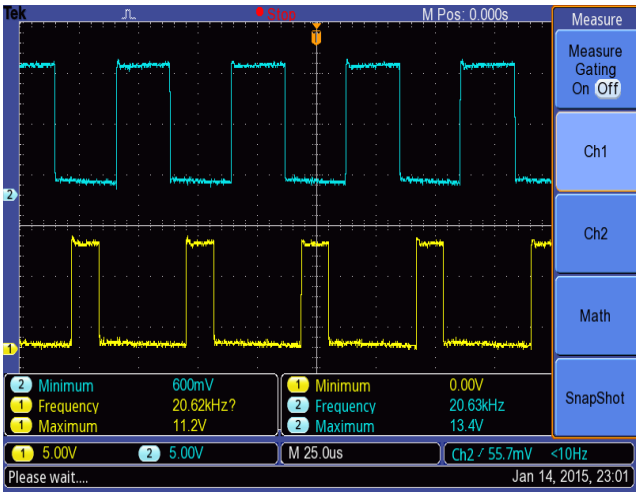

Fig. 21(a). Firing signals of S1 and S2.

The Firing signals of S1 and S2 shown in Fig. 20 are laboratory switching signals for firing power switches S1 and S2. This is observed from the oscilloscope display in Fig. 20. They have frequency of 20.62 kHz and an amplitude of 13.4V. Moreover, the delay gaps between the two complimentary signals are equally shown. Fig. 21(b) clearly illustrates the switching signals that turn ON and OFF at the second leg of the single phase boost differential inverter.

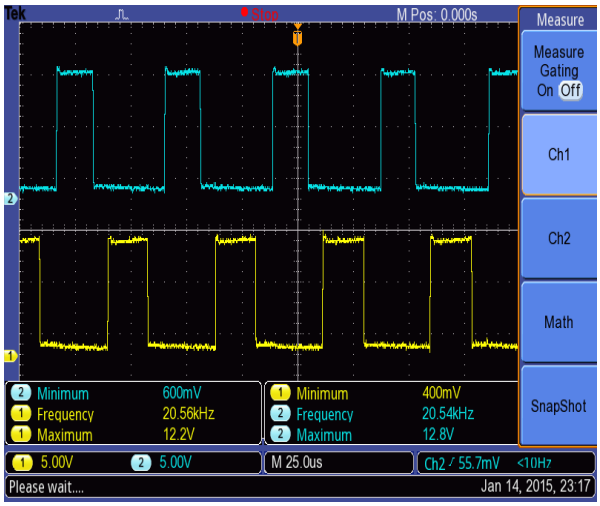

Fig. 21(b). Triggering signals of S3 and S4.

It was observed that the upper signal on the second channel has a frequency of 20.54 kHz and an amplitude voltage of 12.8V; and the lower signal on the first channel of the scope has frequency of 20.56 kHz and an amplitude voltage of 12.2V. This implies that the power switches on the same leg cannot be short-circuited. This is because the signal controlling the upper switches is delayed by 0.01ms.

5.5. Solar Power Station

The solar power generating station used is located at the Department of Electrical Engineering, University of Nigeria, Nsukka at a Latitude of 6.8673° N and Longitude of 7.4085° E.

Fig. 22 shows how the solar transmission cable is run from the generating station into the laboratory where this work was carried out. It can be noticed that the cables are not touching the ground to avoid rodents from attacking it as well as from human beings.

Fig. 22. Solar power Station.

A characterization wooden rectangular box of length 30.00cm and width of 23.00cm is shown in Fig. 23.

Fig. 23. Characterization wooden rectangular box.

It is a part of the solar system that joins the output of solar panels and the power circuit of the proposed system. It is also the section where the solar output voltage and current are measured using two digital multi-meters. The first one situated on the left hand side measures the output current of the solar active connected solar panels, while the second digital multi-meter, determines the voltage output of the solar panels. It can be observed that the ammeter recorded 5.13A when the voltage output of the solar panel is 140V by 10:59am on a sunny day. At the time the solar panels were supplying 5.13A and 140 V, the battery network recorded 48V as displayed in Fig. 23. It shows that the load is fed by the solar panels and not from the battery section. Whenever the solar output voltage is lower than 48V, automatically, the battery voltage supplies the load through the inverter system. The batteries voltage level is shown in Fig. 24.

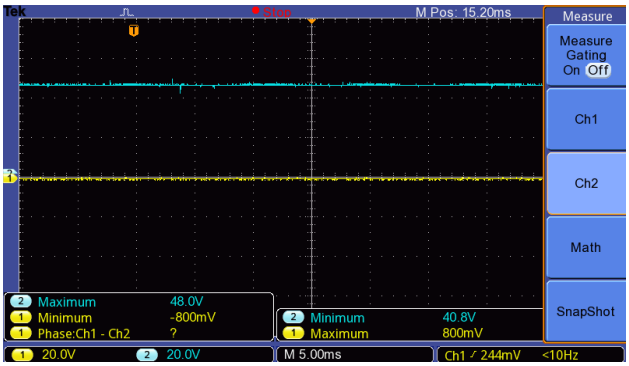

Fig. 24. Level of battery network voltage.

Fig. 24 displayed only when the system was driven in open –loop mode. The idea here is to get the actual DC reference point and AC reference level for controlling the battery banks as well as the DC-AC converter. The name of the oscilloscope used in this research is two-channel Tektronix TBS 1052B 50MHz.

After getting both the DC and AC reference points, we continued the design and implementation of the close loop system by building the feedback system based on the magnitudes of the two references practically.

The pure AC sine wave output voltage of the proposed system is extracted with the aid of USB flash drive and displayed in shown in Fig. 25.

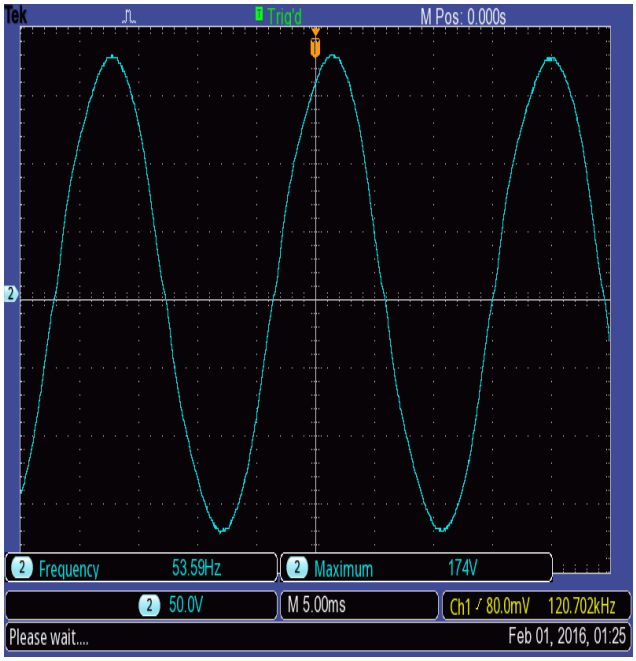

Fig. 25. The output of single phase boost differential inverter.

Fig. 25 shows the pure sinewave output signal of the single phase boost differential inverter. It was observed that the maximum voltage of the pure sinewave from the oscilloscope is 194V which gives us 388V peak-to-peak voltage. In addition, the rms voltage of 194V is reduced to 148V. This system comfortably gives 230V rms value, but the value shown on the oscilloscope in Fig. 25 is the maximum achieved at 50V per division. The limitation of the oscilloscope is that beyond this division, the results are not seen clearly. The

developed Uninterruptible DC-powered boost differential inverter with Sensor-less Changeover system in a closed-loop system is presented in Fig. 26.

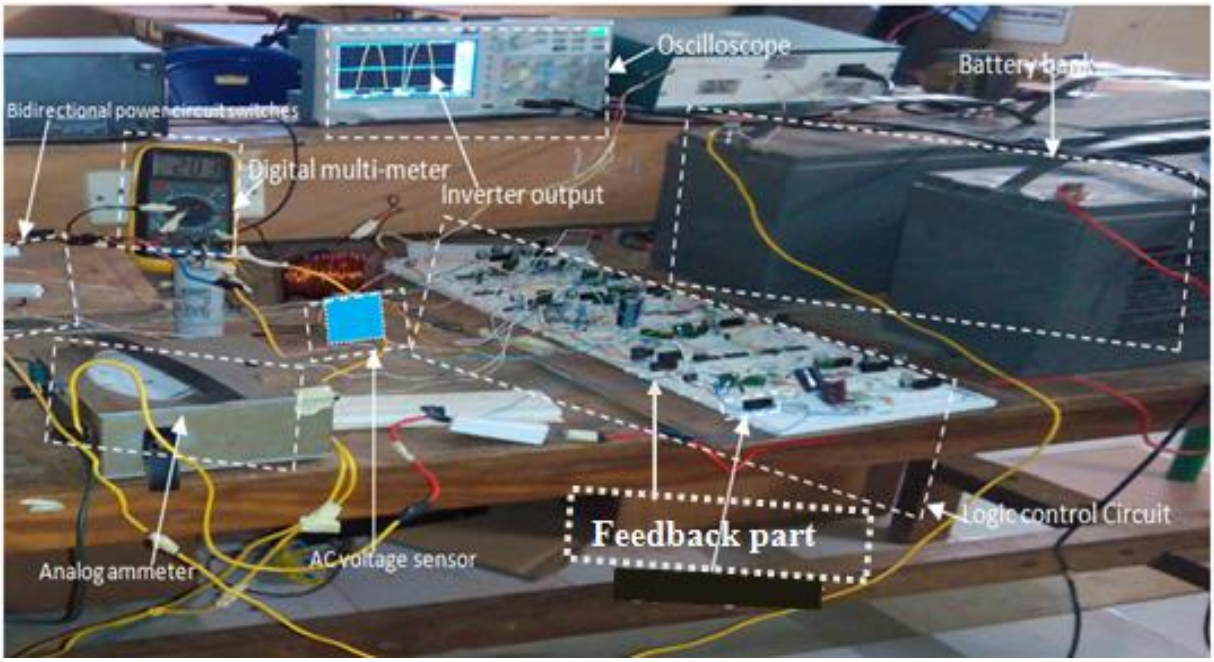

Fig. 27. Uninterruptible DC-powered boost differential inverter with Sensor-less Changeover system in closed-loop system.

6. Conclusion

An uninterruptible DC-powered boost differential inverter with Sensor-less changeover system has been presented, analyzed, simulated, and experimented. The results show that the developed system is efficient, giving an efficiency of 94.4% with a fast dynamic response. The system requires a small amount of power with a power rating of 1 kilowatt. This specification finds application in powering residential areas and medium scale industries.

References

[1] Nnodim, O., Nigeria's power sector losses growing at N474 billion annually. Punch Newspaper, 2019.

[2] Ayamolowo, O.J., Buraimoh, E., Salau, A.O., and Dada, J.O., Nigeria Electricity Power Supply System: The Past, Present and the Future. *2019 IEEE PES/IAS PowerAfrica*, 2019. DOI: 10.1109/powerafrica.2019.8928767

[3] Aamit M. and Kim H., Non-isolated single phase uninterruptible power supply system, *8th International Conference on Power Electronic* (ECCE), Asia, 2011, pp. 2282-2289.

[4] Gupta, B.R. and Singhal, C., Power Electronics. S.K kataria and Sons, 6th Edition New Delhi, 2006, pp. 426-427.

[5] Salau, A.O., Ejidokun, A.O., Adewara, O., Ajala, O.S., Aliyu, E., and Yesufu, T.K., A gsm-based sms power notification system for network operation centers, *Int. J. Sci. Eng. Res. (IJSER),* Vol. 8, No. 7, 2017, pp. 830–837.

[6] Amac, A.E. and Emadi, A., Uninterrupted power supplies, The Electrical Engineering Handbook - Six Volume Set, Third Edition, 2018, pp. 9-73.

[7] Caceres, R.O. and Barbi, I., A boost DC-AC converter, analysis, design, and experimentation, *IEEE Transactions on Power Electronics*, Vol. 14, No. 1, 1999, pp. 134-141.

[8] Akhter, R. and Hoque, A., Analysis of PWM Boost inverter for solar home application, *Internal Conference Enformatika*, 2006, pp. 212-216.

[9] Odeh, C.I., Three-Phase boost DC-AC converter using sliding mode controller, *Nigerian Journal of Technology*, Vol. 30, No. 1, 2011, 20p.

[10] Zhu, G., Tan, S., cheu Y., and Tse, C.K., Mitigation of low-frequency current ripple in fuel-cell inverter systems through waveform control, *IEEE Transactions on Power Electronics,* Vol. 28, No. 2, 2013, pp. 779-791.

[11] Salau, A. O., Eya, C. U., and Onyebuchi, O. C., Nonzero Staircase Modulation Scheme for Switching DC-DC Boost Converter*, Journal of Control Science and Engineering,* 2020, pp. 1–15. DOI: 10.1155/2020/8347462

[12] Mezaroba, M., Giacomini, P.G., de Sousa A.H., and de Souza Margue, L.C., Digital sliding mode controlled three-phase boost inverter implemented in TMS320F2812, *Conferencia Internacional de Aplicacoes Industrial,* Bahia-Brazil, 2006, pp. 6-13.

[13] Koushiki, B. and Ghaisari, J., A voltage reference design for three-phase Boost inverter. *EUROCON,* St.-Petersburg, 2009, pp. 650-654. DOI: 10.1109/EURCON.2009.5167702.

[14] Eya, C., Crescent, O., Ukwejeh, J.M., Solar-powered five level output voltage of dc-to-ac converter using simplified capacitor voltage controlled scheme (SCVCS), *IEEE PES/IAS PowerAfrica*, Abuja, Nigeria, 2019, pp. 1-6. DOI: 10.1109/PowerAfrica46609.2019.9078670.

[15] Li, D., Notohara, Y., Iwaji, Y., and Kurita, Y., AC Voltage and Current Sensorless Control Method for Three-Phase PWM Converter, *Electrical Engineering in Japan*, Vol. 172, No. 4, 2010, pp. 48-57.

[16] Agu, M.U., principles of power electronics circuits, 1st Edition University of Nigeria Press ltd, 2019.

Declarations

Availability of data and material: Not applicable

Code availability: Not applicable

Acknowledgements: Not applicable

Contribution of Individual Authors to the Creation of a Scientific Article (Ghostwriting Policy)

Both CUE formulated the idea, carried out simulations, and wrote some parts of the paper, while AOS provided the method, carried out simulations, and wrote some part of the results and discussion section. SEO analysed the results and wrote part of the results and discussion. All authors have read and approved the manuscript.

Sources of Funding for Research Presented in a Scientific Article or Scientific Article Itself

Authors declare no funding for this research

Conflict of Interest

The authors declare that they have no **conflict of interest**